The EMBO Journal (2008) 27, 1513–1524 | © 2008 European Molecular Biology Organization | All Rights Reserved 0261-4189/08
www.embojournal.org

THE EMBO JOURNAL

Topoisomerase IIIα is required for normal proliferation and telomere stability in alternative lengthening of telomeres

Nassima Temime-Smaali[1,7], Lionel Guittat[1,2,7], Thomas Wenner[1,7], Emilie Bayart[3], Céline Douarre[1], Dennis Gomez[4], Marie-Josèphe Giraud-Panis[5], Arturo Londono-Vallejo[6], Eric Gilson[5], Mounira Amor-Guéret[3] and Jean-François Riou[1,2,*]

[1]Laboratoire d'Onco-Pharmacologie, JE 2428, UFR de Pharmacie, Université de Reims Champagne-Ardenne, Reims, France, [2]Laboratoire de Régulation et dynamique des génomes, INSERM U565, CNRS UMR5153, Muséum National d'Histoire Naturelle USM503, Paris, France, [3]Institut Curie, Section de Recherche, CNRS UMR 2027, Centre Universitaire, Orsay, France, [4]Institut de Pharmacologie et de Biologie Structurale, CNRS UMR 5089, Toulouse, France, [5]Laboratoire de Biologie Moléculaire de la Cellule, CNRS UMR 5239, Ecole Normale Supérieure de Lyon, Lyon, France and [6]Laboratoire Télomères et Cancer, CNRS UMR 7147, Institut Curie, Paris, France

Topoisomerase (Topo) IIIα associates with BLM helicase, which is proposed to be important in the alternative lengthening of telomeres (ALT) pathway that allows telomere recombination in the absence of telomerase. Here, we show that human Topo IIIα colocalizes with telomeric proteins at ALT-associated promyelocytic bodies from ALT cells. In these cells, Topo IIIα immunoprecipitated with telomere binding protein (TRF) 2 and BLM and was shown to be associated with telomeric DNA by chromatin immunoprecipitation, suggesting that these proteins form a complex at telomere sequences. Topo IIIα depletion by small interfering RNA reduced ALT cell survival, but did not affect telomerase-positive cell lines. Moreover, repression of Topo IIIα expression in ALT cells reduced the levels of TRF2 and BLM proteins, provoked a strong increase in the formation of anaphase bridges, induced the degradation of the G-overhang signal, and resulted in the appearance of DNA damage at telomeres. In contrast, telomere maintenance and TRF2 levels were unaffected in telomerase-positive cells. We conclude that Topo IIIα is an important telomere-associated factor, essential for telomere maintenance and chromosome stability in ALT cells, and speculate on its potential mechanistic function.

The EMBO Journal (2008) **27,** 1513–1524. doi:10.1038/emboj.2008.74; Published online 17 April 2008
Subject Categories: genome stability & dynamics; differentiation & death
Keywords: ALT; BLM; G-overhang; telomere; topoisomerase; TRF2

*Corresponding author. Laboratoire de Régulation et dynamique des génomes, INSERM U565, CNRS UMR5153, Muséum National d'Histoire Naturelle USM503, 43 rue Cuvier, CP26, 75231 Paris Cedex 5, France. Tel.: +33 1 40 79 36 98; Fax: +33 1 40 79 37 05; E-mail: riou@mnhn.fr
[7]These authors contributed equally to this work

Received: 12 July 2007; accepted: 19 March 2008; published online: 17 April 2008

Introduction

DNA topoisomerases (Topo) are ubiquitous enzymes that are required for nearly all aspects of DNA metabolism (Wang, 1996; Nitiss, 1998; Champoux, 2001). DNA topoisomerases induce transient breaks in DNA that are associated with a covalent topoisomerase/DNA complex to allow strand passage or enzyme swivelling, which results in the topological state modification of DNA. DNA topoisomerases are divided into four groups, type IA, IB, IIA, and IIB (Wang, 2002). Type IA DNA topoisomerases are conserved in all organisms and function to remove highly negative supercoils; they are assumed to have a fundamental role in the regulation of the topology of replication and recombination intermediates (Wu and Hickson, 2001; Wang, 2002). The budding yeast *Saccharomyces cerevisiae* expresses a single type IA topoisomerase encoded by the *TOP3* gene, initially identified in the *top3*Δ strain by a slow growth phenotype and hyper-recombination between repetitive DNA sequences, such as rDNA (Wallis *et al*, 1989). The deletion of *SGS1*, whose product belongs to the RecQ family of DNA helicases involved in the maintenance of genome stability, suppresses the *TOP3* loss-of-function phenotype. It was subsequently shown that Sgs1p forms a complex with Top3p (Gangloff *et al*, 1994; Hickson, 2003).

Humans have two members of the IA subfamily, Topo IIIα and Topo IIIβ (Wang, 2002). Topo IIIα exists in a complex with BLM, a RecQ helicase whose mutation is responsible for Bloom's syndrome (BS) (Johnson *et al*, 2000; Wu *et al*, 2000). In biochemical assays, Topo IIIα has a weak DNA relaxation activity on double-stranded DNA but is able to bind, cleave, and religate single-stranded DNA (Goulaouic *et al*, 1999). The interaction of BLM with Topo IIIα stimulates the strand passage activity of Topo IIIα (Wu and Hickson, 2002). Furthermore, Topo IIIα and BLM cooperate to convert double Holliday junctions (DHJ) to decatenated products *in vitro*, suggesting a putative role of the complex in the resolution of recombination intermediates (Wu and Hickson, 2003). Recently, BLAP75/RMI1 was identified as a third component of the BLM/Topo IIIα complex; this protein is also highly conserved among eukaryotes (Chang *et al*, 2005; Yin *et al*, 2005). BLAP75/RMI1 recruits Topo IIIα to DHJ and its depletion by RNA interference increases the frequency of sister chromatid exchanges (Yin *et al*, 2005; Wu *et al*, 2006). Under normal cell growth conditions, BLM and Topo IIIα colocalized in promyelocytic (PML) nuclear bodies together with many other proteins, including Rad50, Mre11, NBS1, p53, and Sp100 (Johnson *et al*, 2000; Yankiwski *et al*, 2000), and this localization is disrupted in BS cells (Johnson *et al*, 2000). The Topo IIIα/BLM complex was also proposed to function as a repair complex in response to replication defects and may restart stalled replication forks (Ababou *et al*, 2000; Wang *et al*, 2000; Amor-Gueret, 2006). Following camptothecin treatment, a phosphorylated form of BLM dissociates from

the Topo IIIα/BLM complex at its PML storage sites and accumulates with γ-H2AX at replication damage sites (Rao *et al*, 2005).

Telomeres consist of repetitive G-rich DNA sequences that protect the chromosome ends from fusion and illegitimate recombination. In human somatic cells, telomere length decreases at each round of division and cellular mechanisms that counteract this degradation are able to confer indefinite proliferation potential. Two classes of mechanisms have been described in human tumor cells that allow the maintenance of telomere length. The first requires a specialized enzyme, called telomerase, which is able to copy, as a reverse transcriptase, the short TTAGGG motif at the 3′ end of telomeres. Telomerase is composed of a catalytic subunit, hTERT, associated with an RNA containing the template of the telomere repeat unit, hTR. Telomerase is overexpressed in a large number of tumours (about 85%) and is involved in the capping of telomere ends (McEachern *et al*, 2000). The second mechanism is observed in tumours (about 15%) as well as in immortalized cell lines lacking telomerase activity and involves recombination between telomeres, a mechanism known as alternative lengthening of telomeres (ALT) (Dunham *et al*, 2000; Londono-Vallejo *et al*, 2004). ALT cells display a heterogeneous telomere length and particular nuclear foci termed ALT-associated PML bodies (APB) that contain, in addition to PML, telomeric DNA, telomere binding proteins (TRF1 and TRF2), and several proteins involved in DNA synthesis, repair, and recombination. The latter include the MRE11/RAD50/NBS1 complex and the RecQ helicases WRN and BLM (Kim *et al*, 1995; Yeager *et al*, 1999; Grobelny *et al*, 2000; Wu *et al*, 2000; Huang *et al*, 2001; Lillard-Wetherell *et al*, 2004; Tsai *et al*, 2006). In yeast, telomerase-negative survivors with heterogeneous telomere sequences (type II) also involve a telomere–telomere recombination mechanism that requires Rad50p, Rad52p, and Sgs1p (Huang *et al*, 2001) as well as Top3 (Kim *et al*, 1995; Tsai *et al*, 2006).

Telomeres end in a 3′ single-stranded overhang that may be involved in different DNA conformations such as t-loop and/or G-quadruplexes (Mergny *et al*, 2002; de Lange, 2005). T-loops are created through strand invasion of the 3′ telomeric overhang into the duplex part of the telomere and are thought to represent a strategy to protect chromosome ends. They might also correspond to recombination intermediates. TRF2 is required for the establishment of t-loops and these structures are presumably involved in protecting the DNA at the telomeric single/double-strand junction (de Lange, 2005). RecQ helicases associated with the telomeric complex, such as WRN or BLM (Lillard-Wetherell *et al*, 2004), cooperate with POT1 (protection of telomere 1), a protein that binds specifically to the single-strand telomeric sequence, to unwind telomeric forked duplexes and D-loop structures (Opresko *et al*, 2005).

Therefore, Topo IIIα might participate in solving topological issues arising from the action of a RecQ helicase during telomere recombination/replication in the ALT pathway. We have examined whether Topo IIIα is required for the correct maintenance of telomeres of ALT and telomerase-positive cells. We show that Topo IIIα interacts with TRF2 independently of its interaction with BLM and forms a complex with TRF2 and BLM at APB in ALT cells. Topo IIIα interacts with telomeric DNA as shown by chromatin immunoprecipitation (ChIP) assays in ALT cells and its depletion by small interfering RNA (siRNA) leads to the accumulation of anaphase bridges and to telomere uncapping and is associated with cell growth arrest. As Topo IIIα interacts *in vitro* with single-stranded telomeric sequences, we suggest that the BLM/Topo IIIα/TRF2 complex at APB is involved in the maintenance of telomeres in ALT cells, possibly through the resolution of intermediate DNA structures that arise during telomere recombination.

Results

Colocalization of Topo IIIα at APB with PML and shelterin subunits in ALT cells

Indirect immunofluorescence staining with an anti-Topo IIIα antibody detected Topo IIIα protein organized into multiple nuclear foci in the ALT cell lines WI38-VA13, MRC5-V1, and U2OS (Figure 1A and Supplementary Figure S1A). Antibodies that recognize the human TRF2 and PML proteins were used to identify APB in these cells. Topo IIIα foci were large and bright and an almost complete colocalization (>90%) of Topo IIIα, TRF2, and PML was observed (Figure 1A and Supplementary Figure S1A). To confirm that Topo IIIα is a component of APB, MRC5-V1 cells were stably transfected with YFP–Topo IIIα and stained with TRF2 or PML antibodies (Figure 1B and D) or cotransfected with other CFP-tagged shelterin components (CFP–TRF2, CFP–POT1, or CFP–TIN2) (Figure 1C and D). The results showed a strong colocalization of YFP–Topo IIIα, POT1, TIN2, TRF2, and PML in agreement with the indirect immunofluorescence results. Similar experiments were performed in two telomerase-positive cell lines (EcR293 and HT1080) and indicated that YFP–Topo IIIα perfectly colocalizes with PML (Supplementary Figure S1B). In contrast to ALT cells, only rare colocalizations were observed between TRF2 foci and YFP–Topo IIIα in interphase nuclei from telomerase-positive cells (Figure 1C, arrows, and Supplementary Figure S2). During mitosis, the Topo IIIα signal is absent from condensed chromosomes in both ALT and telomerase-positive cells (Supplementary Figure S2). These results indicate that Topo IIIα is localized at APB in ALT cells. In contrast, Topo IIIα foci mostly correspond to PML foci in telomerase-positive cells in agreement with previous studies (Johnson *et al*, 2000; Wu *et al*, 2000).

Topo IIIα interacts with TRF2

To test for a physical interaction between telomeric proteins and Topo IIIα, we performed co-immunoprecipitation experiments in U20S, MRC5-V1 ALT, HT1080, and 293T telomerase-positive cell extracts. In the complex precipitated by the Topo IIIα D6 antibody, we detected TRF2 by immunoblotting (Figure 2). A similar result was obtained for EcR293 telomerase-positive cells and WI38-VA13 ALT cells (data not shown). Immunoblotting with an anti-BLM antibody also revealed the presence of BLM in the Topo IIIα complex (data not shown). To investigate this further, the reverse experiments using an anti-TRF2 antibody was performed in telomerase-positive and ALT cells (Figure 2). For unknown reason that could include the presence of the epitope close to the protein interaction region or the relative abundance of these proteins in nuclei, we were unable to reproducibly co-immunoprecipitate Topo IIIα using TRF2 antibody (Figure 2 and data not shown). Despite modifications of the immuno-

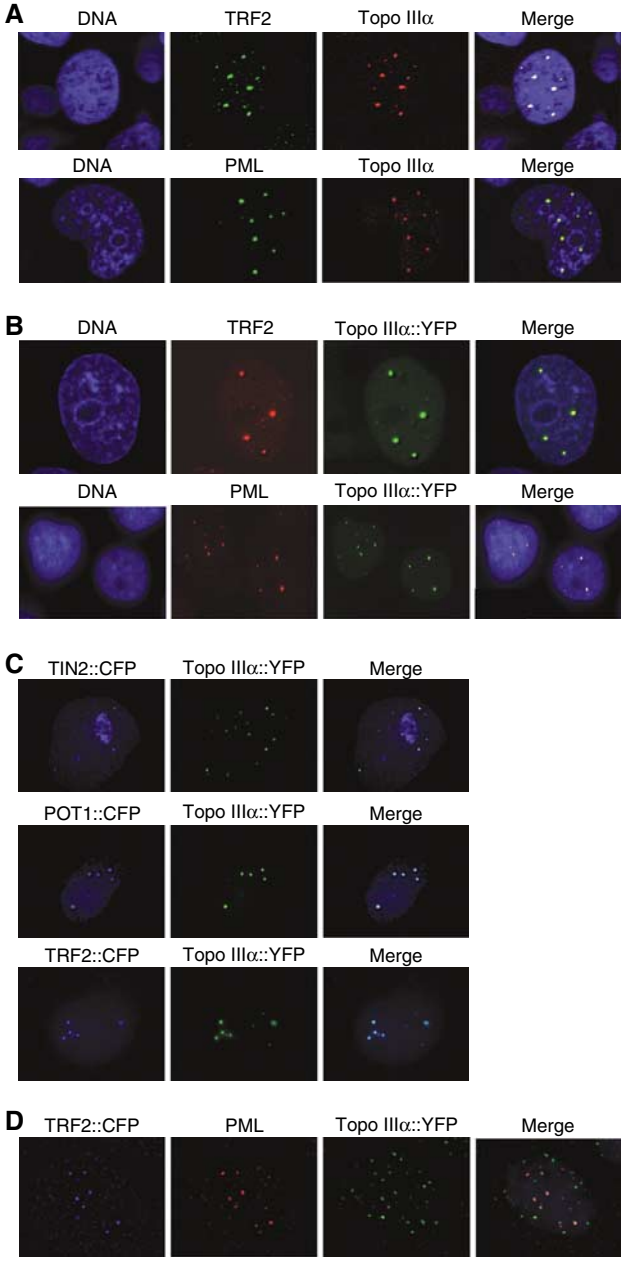

Figure 1 Topo IIIα colocalizes with PML and shelterin components at APB in MRC5-V1 ALT cells. The stable expression of a YFP-tagged Topo IIIα protein was also used to determine its localization. (**A**) Colocalization of Topo IIIα (red, detected by immunofluorescence) with TRF2 or PML (green, detected by immunofluorescence. (**B**) Representative images of colocalization in MRC5-V1 of Topo IIIα tagged with YFP (Topo IIIα::YFP, green), with TRF2 or PML (red, detected by immunofluorescence). (**C**) Representative images of colocalization in MRC5-V1 of Topo IIIα tagged with YFP (Topo IIIα::YFP, green) with TIN2 tagged with CFP (blue, TIN2::CFP), POT1 tagged with CFP (blue, POT1::CFP), or TRF2 tagged with CFP (blue, TRF2::CFP). (**D**) Representative images of colocalization in MRC5-V1 of Topo IIIα tagged with YFP (Topo IIIα::YFP, green), TRF2 tagged with CFP (TRF2::CFP, blue), and PML (red detected by immunofluorescence).

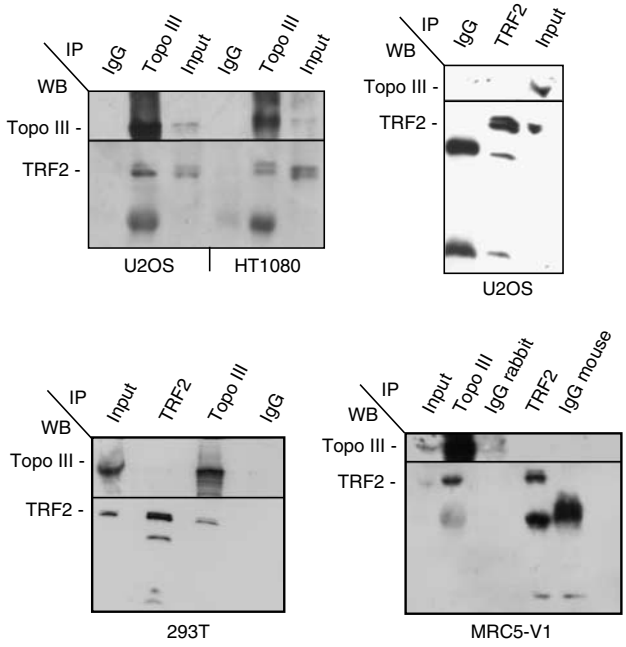

Figure 2 Topo IIIα/TRF2 complex is detected in telomerase-positive and ALT cells as revealed by immunoprecipitation with D6 Topo IIIα antibody. The antibodies (TRF2, Topo III, or control IgG) used for immunoprecipitation (IP) are listed at the top of each panel and the antibodies (BLM, Topo III, and TRF2) used for western blot analysis (WB) are listed at the left of each panel. Topo IIIα co-immunoprecipitates TRF2 in HT1080 or 293T (telomerase-positive) and in U2OS or MRC5-V1 (ALT) cell lines. Reciprocal immunoprecipitation of Topo IIIα by TRF2 antibody (4A794, mouse) is not detected in 293T, U2OS, or MRC5-V1 and is unreproducible in other cells.

precipitation protocol using milder detergent conditions, the use of nuclear extract, and the use of other TRF2 antibodies, we were unable to recover significant amounts of Topo IIIα in TRF2 immunoprecipitates (Supplementary Figure S3).

Next, we investigated whether the BLM/Topo IIIα/TRF2 complex depended on the presence of DNA by evaluating its resistance to DNase treatment. The MRC5-V1 protein extract was treated with DNase I (data not shown). This treatment did not impair the recovery of TRF2 and BLM from Topo IIIα immunoprecipitates, suggesting the existence of DNA-independent interactions among BLM, Topo IIIα, and TRF2 in ALT cells.

We further determined whether the TRF2/Topo IIIα complex was stable in the absence of the BLM protein by using the telomerase-positive and BLM-deficient GM08505 cell line (data not shown). Immunoprecipitation experiments indicated that TRF2 and Topo IIIα interacted, suggesting that these two proteins form a BLM-independent complex. Thus, we concluded that the presence of BLM is not required for Topo IIIα/TRF2 interaction.

These data suggest that the Topo IIIα/TRF2 complex might exist as part of a multiprotein complex in telomerase-positive and ALT cells.

Topo IIIα associates with telomeric DNA in ALT cells

Next, we studied the *in vitro* interaction of purified recombinant Topo IIIα (Goulaouic *et al*, 1999) with telomeric DNA by electrophoretic mobility shift assay (EMSA) using oligonucleotides corresponding to double-stranded telomeric repeats with a 3′ G-rich single-stranded extension (Tel-1) or without the single-stranded region (Tel-2) (Figure 3). Gel shift assays with increasing concentrations of Topo IIIα were performed

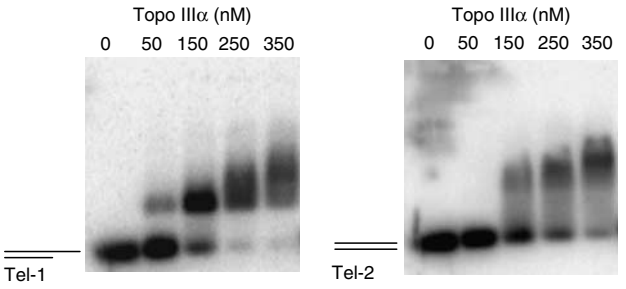

Figure 3 Topo IIIα interacts with telomeric sequences *in vitro*. EMSA were performed using 5 nM of telomeric template with a 3′ single-stranded extension (Tel-1, left panel) or without the single-stranded region (Tel-2, right panel) (see Materials and methods for details) in the presence of increasing concentrations (50, 150, 250, and 350 nM) of purified recombinant Topo IIIα (Goulaouic *et al*, 1999). For Tel-1, a Topo IIIα/DNA bandshift was detected at 50 nM, whereas the Tel-2/Topo IIIα bandshift was detected at 150 nM, suggesting a preferential binding to the 3′ single-stranded extension.

in the presence of 5 nM of radiolabelled oligonucleotide. Topo IIIα bound to the telomeric substrate with a 3′ G-overhang (Tel-1) with a band shift detectable at a concentration as low as 50 nM (Figure 3, left panel). Under the same experimental conditions, a Topo IIIα band shift was detected on the DNA substrate without the G-overhang extension (Tel-2) at a concentration equal to 150 nM (Figure 3, right panel), suggesting that Topo IIIα bound to the G-overhang sequence, in agreement with the known preference of Topo IIIα for single-stranded DNA (Goulaouic *et al*, 1999; Chen and Brill, 2007). To determine whether TRF2 and Topo IIIα form a complex at single-stranded telomeric DNA, retardation assays were also performed using the 21G oligonucleotide (Supplementary Figure S4). Owing to its short size (21 nucleotides), the binding of Topo III or TRF2 requires higher protein concentrations (>350 nM). The addition of Topo IIIα and TRF2 induces the formation of a higher molecular weight complex (see arrow), suggesting the formation of a ternary Topo IIIα/TRF2/DNA complex. A similar result was obtained with the 21Gmu3 oligonucleotide in which three guanines of the telomeric sequence have been replaced by cytosines (Supplementary Figure S4), indicating that the complex formation is not sequence dependent. A ternary complex was also obtained using the double-stranded DS26 oligonucleotide (Supplementary Figure S4, arrow). In these conditions, the binding of TRF2 on this nontelomeric sequence is nearly undetectable, indicating that Topo IIIα recruits TRF2 onto DNA by direct interaction.

To evaluate whether Topo IIIα is associated with telomeric DNA, ChIP experiments were performed in ALT and telomerase-positive cells (293T, HeLa, HT1080, MRC5-V1, U2OS, and WI38-VA13). In a first set of experiments, telomeric DNA immunoprecipitated by Topo IIIα was analysed by PCR amplification (Cawthon, 2002) and a smear indicative of telomeric DNA was detected in all cell lines tested (result not shown).

Determination of the relative Topo IIIα amount at the telomere, as compared to other repeated sequences in the genome, was performed using a dot blot hybridization assay using telomeric and Alu repeat probes in 293T, MRC5V1, and U2OS cells (Figure 4). TRF2 was used as a positive control. The results indicated that the amount of telomeric DNA recovered by TRF2 immunoprecipitation was nearly

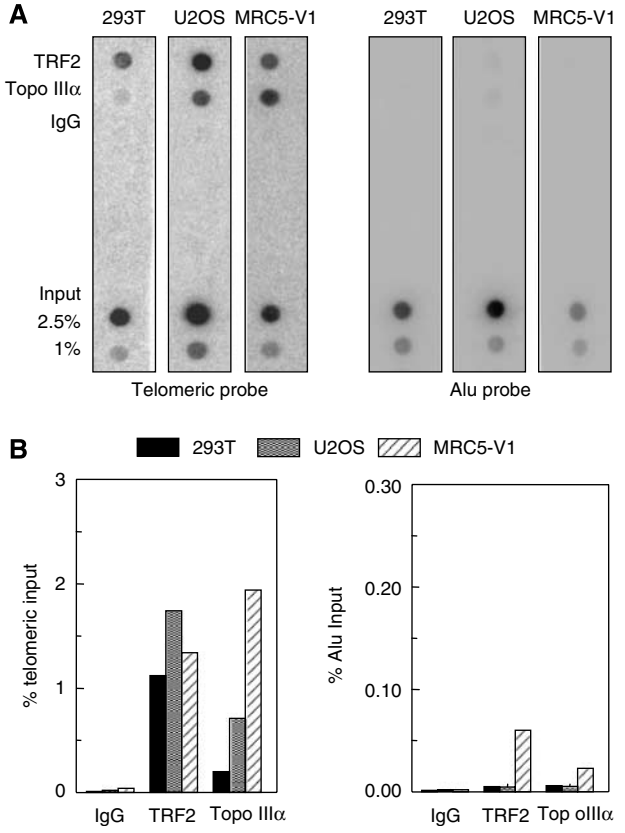

Figure 4 Topo IIIα interacts with telomeric sequences *in vivo* as shown by ChIP. Three different cell lines (telomerase-positive 293T and MRC5-V1 and U2OS ALT cell lines) were evaluated after ChIP with TRF2 or Topo IIIα antibodies. IgG antibodies were used as negative controls. Total input fractions (2.5 and 1%) and antibody-recovered fractions (10% of input) were subjected to Southern blot analysis using telomeric or ALU repeat-specific probes. (**A**) Representative ChIP experiment. (**B**) Quantification of radioactivity by Imagequant™ software of the experiment presented in (A). The percentage of precipitated DNA was calculated as a ratio of input (telomeric or Alu) signals and plotted.

equivalent in the telomerase-positive and ALT cell lines (Figure 4B and data not shown). In contrast, the amount of telomeric DNA recovered by Topo IIIα immunoprecipitation was higher in ALT cells than in 293T cell line, and corresponded to a specific association with telomeric sequence when compared to Alu (Figure 4A and B). The relative increase of telomeric DNA immunoprecipitation by Topo IIIα in ALT cells, as compared to 293T (defined as 1), was equal to 3.2±0.7-fold for U2OS and 5.6±2.9-fold for MRC5-V1 (Figure 4B and data not shown). These data suggest that Topo IIIα has a marked preference for telomeric DNA in ALT cells. As a hallmark of ALT cells is their extreme heterogeneity in telomere length due to homologous recombination and the presence of extra chromosomal telomeric repeats (ECTR or t-circles) (Dunham *et al*, 2000; Cesare and Griffith, 2004; Londono-Vallejo *et al*, 2004; Wang *et al*, 2004), we cannot exclude the possibility that the increased ratio of Topo IIIα at telomeric DNA relative to Alu DNA in ALT cells was due to binding to ECTR rather than to telomeres.

siRNA directed against Topo IIIα inhibits ALT cell growth

To examine the importance of Topo IIIα for ALT cell growth, Topo IIIα gene expression was downregulated by

RNA interference using specific siRNA oligonucleotide duplexes. Three siRNAs, Si-1, Si-2, and Si-3 Topo IIIα, were designed to target the Topo IIIα cDNA sequence (NM004618) and evaluated for effects on Topo IIIα expression levels in the MRC5-V1 cell line 72 h after siRNA transfection. Immunoblots indicated that the Topo IIIα protein level decreased when cells were treated with Si-1 and Si-2 (60–70%) as compared to the control siRNA (Figure 5A). No significant decrease was observed when cells were treated with Si-3. An evaluation of the time course of the effect of Si-1 in MRC5-V1 cells indicated a marked decrease in Topo IIIα levels at 72–96 h after transfection (76–83%) (Figure 5B).

We next determined the importance of Topo IIIα for the growth of various ALT (MRC5-V1, U2OS, and WI38-VA13) and telomerase-positive (EcR293 and HT1080) cell lines 24–96 h after Si-1 transfection (Figure 5C). In parallel, the efficiency of the Topo IIIα depletion was evaluated by immunoblotting using the anti-Topo IIIα antibody 72 h after transfection (Figure 5C). For the five cell lines tested, the decrease in Topo IIIα protein level ranged from 60 to 80%. Treatment of the three ALT cell lines with Si-1 Topo IIIα induced a strong reduction in cell growth, as compared to control siRNA-treated cells. Growth inhibition began at 48 h after Si-1 transfection. Cell growth inhibition induced by Si-1 treatment was also associated with a reduction in cell viability determined by Trypan blue exclusion, which decreased to 32, 22, and 50% of controls for MRC5-V1, U2OS, and WI-38-VA13 cells, respectively, but without significant induction of apoptosis, measured by PARP1 and caspase-3 cleavage (Supplementary Figure S6).

In contrast, depletion of Topo IIIα by RNA interference using Si-1 in telomerase-positive cell lines (EcR293 and HT1080) did not alter the proliferation of these cells compared to cells treated with control siRNA (Figure 5C). This difference between telomerase-positive and ALT cells was also observed when HT1080 and U2OS cells were treated with Si-2 (Supplementary Figure S5A). These results showed that Topo IIIα is essential for the proliferation of ALT cells but not for telomerase-positive cells over the time course of the assay.

Topo IIIα depletion induces anaphase bridge formation, G-overhang signal decrease, and TRF2 depletion in ALT cells

Telomere binding proteins such as TRF2 and its partners such as TIN2, RAP1, and Apollo have a pivotal role in the maintenance of the integrity of telomeres (de Lange, 2005; Lenain *et al*, 2006; van Overbeek and de Lange, 2006). As our results indicated that Topo IIIα forms a complex with TRF2 in ALT cells, we examined the importance of Topo IIIα for telomere integrity by analysing the formation of anaphase bridges, usually associated with a telomere dysfunction (Figure 6). In MRC5-V1 and U2OS cells transfected with Si-1 (100 nM), a large number of cells containing anaphase bridges were observed (72–87.5% of cells) as compared to those treated with control siRNA (11–17.5%) (Figure 6A). In contrast, the formation of anaphase bridges was similar (17%) in Topo IIIα-depleted HT1080 cells compared to cells treated with control siRNA (15%).

Four different kinds of anomalies during anaphase were distinguished in MRC5-V1 cells treated with the siRNA targeting Topo IIIα (Figure 6B). Anaphase cells with one unique bridge (17%; Figure 6B, panel a), multiple bridges (48%; panel b), quasi-complete entanglement (25%; panel c), and cross-shaped bridges (10%; panel d) were observed after Topo IIIα depletion. These results suggested that chromosome entanglement or telomere dysfunction is induced by Topo IIIα depletion in ALT cells but not in the telomerase-positive HT1080 cells; treatment of telomerase-positive cells with siRNA had no effect on the percentage of cells that contained anaphase bridges. Similar results were obtained using Si-2 Topo IIIα in HT1080 or U2OS cells (Supplementary Figure S5B).

To further study the role of Topo IIIα in the stability or maintenance of the telomere ends, we evaluated the amount of G-overhang telomere DNA in telomerase-positive and ALT cells after treatment with the siRNA targeting Topo IIIα using solution hybridization experiments (Figure 7A and B). Downregulation of Topo IIIα in HT1080 cells had no effect on the G-overhang signal, whereas a strong reduction was observed in ALT cells (MRC5-V1, U2OS, WI38-VA13) ranging from 40 to 60% of the signal from corresponding control siRNA.

As Topo IIIα, BLM, and TRF2 can form a complex, we investigated whether Topo IIIα depletion had an effect on the BLM and TRF2 protein levels. Western blot analysis for Topo IIIα, BLM, and TRF2 proteins was performed on cells treated with Si-1 72 h after transfection (Figure 7C and D). Topo IIIα depletion was associated with a significant decrease in BLM protein levels in telomerase-positive (HT1080) and ALT (MRC5-V1, U2OS) cells, ranging from 36 to 84%. Interestingly, we also observed a decrease in TRF2 protein levels in ALT cells (56–74%) but not in HT1080 cells (2%). These results are consistent with the notion that Topo IIIα, TRF2, and BLM form a complex in ALT cells and that Topo IIIα and TRF2 interact with telomeric sequences. The reduced protein level of TRF2 in ALT cells treated with Si-1 might be responsible for the telomere dysfunction observed in these cells. Similar results were obtained using Si-2 Topo IIIα in HT1080 or U2OS cells (Supplementary Figure S5C).

Topo IIIα depletion induces telomere dysfunction-induced foci in ALT cells

To determine whether Topo IIIα depletion affected telomere integrity, we also tested ALT cells for DNA damage that colocalized with telomeres. Telomere dysfunction-induced foci (TIF) can be detected due to the presence of γ-H2AX, a phosphorylated variant of histone 2A that associates with DNA double-strand breaks. U2OS cells transfected with Si-1 were analysed after 48 h for γ-H2AX-containing foci that colocalized with TRF1. There was a low level of γ-H2AX foci in control U2OS cells (11.2 ± 2.5 foci/nuclei) with only 5.6 ± 0.5 colocalizing with TRF1 (Figure 8), in agreement with previous observations (Nabetani *et al*, 2004). Consistent with G-overhang shortening and telomere uncapping (TRF2 loss), in Si-1-treated cells we observed an increased number of γ-H2AX foci (48.8 ± 8.7 foci/nuclei) with 49.7 ± 9.3% colocalizing with TRF1 (Figure 8), suggesting that Topo IIIα depletion triggers a DNA damage response that takes place, at least in part, at telomeres.

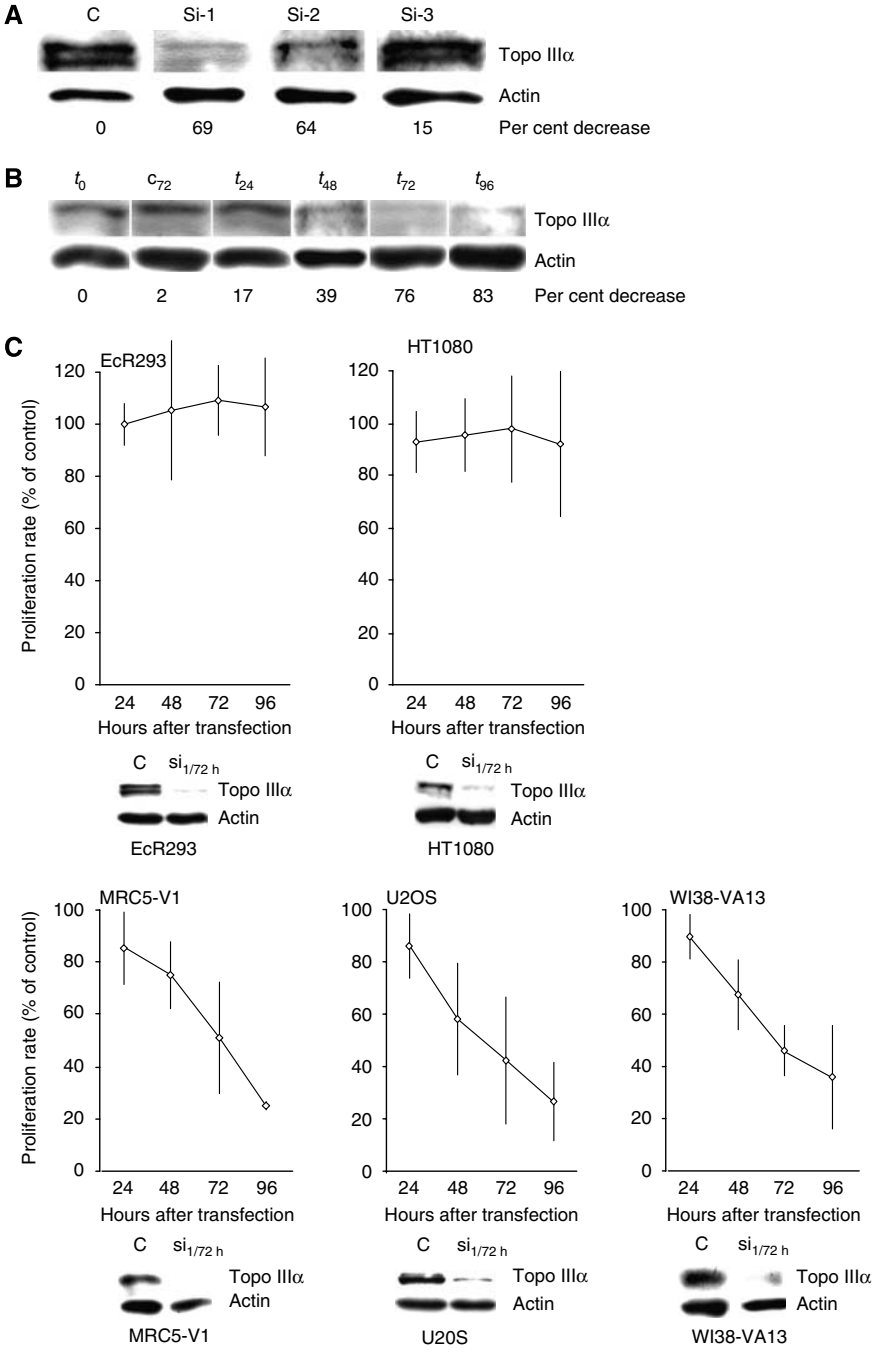

Figure 5 Effect of Topo IIIα depletion by RNA interference on telomerase-positive and ALT cells growth. (**A**) Representative example of effect of three different siRNAs targeting Topo IIIα (Si-1, Si-2, and Si-3; see sequences in Materials and methods) and a control siRNA (C) on the amount of intracellular Topo IIIα protein at 72 h in the MRC5-V1 (ALT) cell line. The loading control was β-actin. The per cent decrease of Topo IIIα compared to treatment with the control is indicated at the bottom. (**B**) Data from a representative experiment in MRC5-V1 (ALT) cell line with Si-1. Negative control siRNA at 72 h (c_{72}) and the amount of Topo IIIα before treatment (t_0) are shown as controls. The per cent decrease of Topo IIIα relative to the control is indicated at the bottom. (**C**) Effect of Topo IIIα depletion (Si-1, 100 nM) on the growth of telomerase-positive (EcR293 and HT1080) and ALT (MRC5-V1, U2OS, and WI38-VA13) cell lines for up to 96 h after transfection. The results are expressed relative to control siRNA-treated cells, defined as 100%, and correspond to the mean value and standard deviation of three independent experiments. As a control for Topo IIIα depletion, a western blot experiment performed in parallel is presented at the bottom of each growth curve. Protein extracts from Si-1-treated cells at 72 h (Si-1/72 h) or from control siRNA-treated cells (C) were blotted using antibodies against Topo IIIα and β-actin.

BLM depletion reduces ALT cell growth but does not modify Topo IIIα or TRF2 protein levels in telomerase-positive and ALT cells

Our results showing that Topo IIIα depletion was associated with a significant decrease in BLM protein levels in telomerase-positive and ALT cells prompted us to check whether BLM depletion has an effect on Topo IIIα or TRF2 protein levels. We thus analysed Topo IIIα and TRF2 protein expression after 48 or 72 h of siRNA-mediated depletion of BLM in HeLa cells or U2OS cells. As shown in Figure 9A,

siRNA-mediated depletion of BLM was very efficient, and we did not detect any change in Topo IIIα or TRF2 protein levels in both BLM-depleted HeLa and U2OS cells. However, BLM depletion significantly reduced the growth of U2OS cells, whereas it did not modify the growth of HeLa cells; growth inhibition of BLM-depleted U2OS cells was clearly detectable as early as 48 h after si-BLM transfection (Figure 9B), but was clearly weaker than the growth inhibition induced by Topo III depletion in U2OS cells (Figure 5C and Supplementary Figure S5A).

Discussion

One important finding of this work is that Topo IIIα is present at telomeric sequences in both ALT and telomerase-positive cells. In ALT cells, ChIP with Topo IIIα antibody indicated that Topo IIIα was preferentially bound to telomeric DNA over Alu sequences and that Topo IIIα colocalized with TRF2 and BLM (Lillard-Wetherell *et al*, 2004). In telomerase-positive cells, there was a lower or no association of Topo IIIα with telomeric chromatin as evaluated by ChIP and by costaining with TRF2, respectively; however, we observed that a significant amount of TRF2 immunoprecipitated with Topo IIIα antibody in both telomerase-positive and ALT cells. The TopoIIIα/TRF2 complex was also detected in BLM-deficient telomerase-positive cells, indicating that the formation of TRF2/TopoIIIα complexes is independent of BLM. Despite evidence of substantial Topo IIIα and TRF2 association in telomerase-positive cells, the significant interaction of Topo IIIα with telomeric sequences by ChIP, together with the interaction with TRF2 observed by immunoprecipitation may suggest a transient function for Topo IIIα during telomere maintenance or replication. On the other hand, we cannot exclude a direct association between TRF2 and Topo IIIα independent of a telomeric context, linked to additional functions of TRF2 in double-strand break repair of DNA (Mao *et al*, 2007). We conclude that Topo IIIα is preferentially recruited to telomeres or at ECTR in ALT cells and that a detectable interaction at telomeric sequences and with TRF2 is also found in telomerase-positive cells, the significance of which remains to be determined.

Our *in vitro* results indicated that Topo IIIα binds better single-stranded than double-stranded telomeric sequence, a result in agreement with the known preference of Topo IIIα for single-stranded DNA. As TRF2 can introduce a torsional stress in telomeric DNA, a process that increases single-stranded bubbles in duplex DNA (Amiard *et al*, 2007), Topo IIIα might have a general role in telomere physiology by resolving TRF2-mediated topological

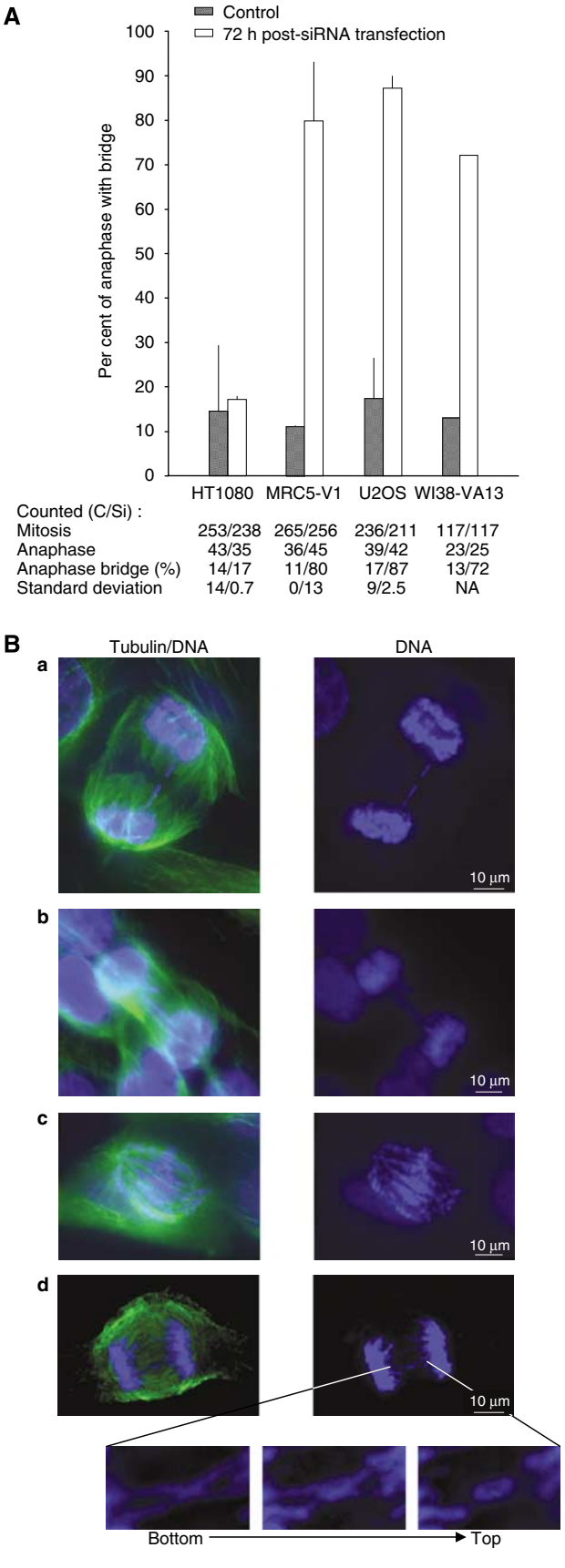

Figure 6 Topo IIIα depletion increases anaphase bridge formation in ALT cell lines. (**A**) Per cent of cells in mitosis harbouring anaphase bridges 72 h after transfection with control siRNA (grey bar) or Si-1 (white bar). Numbers of cells in mitosis and anaphase, percentage of cells with anaphase bridges, and standard deviation are indicated for each cell line for control siRNA (C) and for the siRNA targeting Topo IIIα Si-1 (Si). Experiments were performed in triplicate, except for WI38-VA13 (single determination). NA indicates not applicable. (**B**) Representative images of the types of anaphase bridges observed: (**a**) single anaphase bridge, (**b**) multiple anaphase bridges, (**c**) abnormal anaphase bridges or chromosome entanglements, and (**d**) cross-like anaphase bridges. Cells were immunolabelled with α-tubulin antibody (green; see Materials and methods) and DNA was stained with DAPI (blue). Only the merge pictures (tubulin/DNA) and the DAPI stainings (DNA) are shown. Magnification and z-variation of this structure from the bottom to the top of the cell are shown under the main pictures.

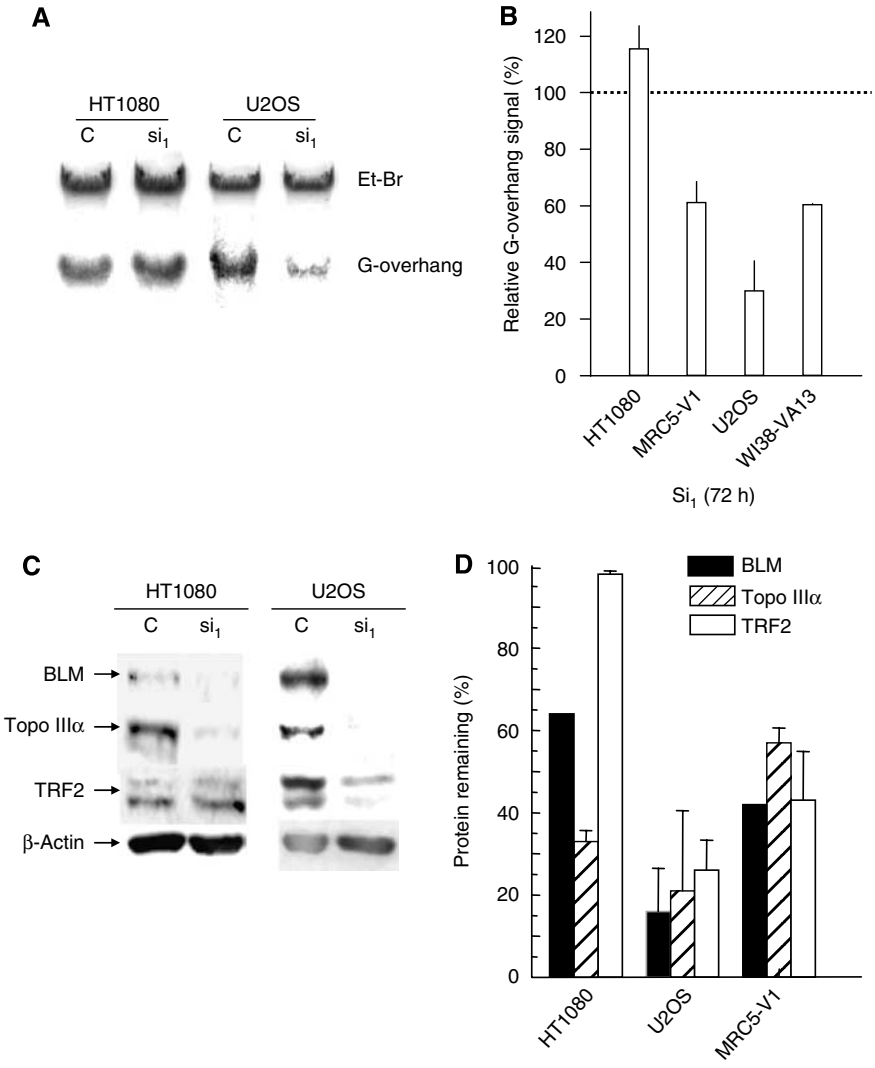

Figure 7 Effect of Topo IIIα depletion on G-overhang signal and stability of the Topo IIIα/BLM/TRF2 complex. (**A**) Representative experiment showing the effect of Topo IIIα depletion on the telomeric G-overhang signal in HT1080 and U2OS cells. DNA was extracted from cells 72 h after transfection with the control siRNA (C) or with Si-1 (si_1). The G-overhang signal was evaluated by nondenaturing solution hybridization with a telomeric probe. G-overhang: signal obtained with the $(AATCCC)_4$ probe; EtBr: ethidium bromide DNA staining in the gel. (**B**) Quantification of the effect of Topo IIIα depletion on the G-overhang signal in four different cell lines. The G-overhang hybridization signal was normalized relative to the EtBr signal. The results are expressed as the percentage of G-overhang signal in control siRNA-transfected cells, defined as 100%. Mean ± s.d. is of three independent experiments, including those presented in (A), except for WI38-VA13 (two experiments). (**C**) Representative experiment showing the effect of Topo IIIα depletion on the stability of the Topo IIIα/BLM/TRF2 complex in HT1080 and U2OS cells by western blot analysis. Cell extracts were prepared 72 h after transfection with the control siRNA (C) or with Si-1 (si_1). (**D**) Quantification of the effect of Topo IIIα depletion on the BLM, TRF2, and Topo IIIα protein levels in HT1080, U20S, and MRC5-V1 cell lines. The results are expressed as the percentage of protein level remaining relative to control siRNA-treated cells. Mean ± s.d. is of three independent experiments, including those presented in (C).

intermediates. This topological function may explain the transient association of this enzyme with telomeric DNA. TRF2 is known to be recruited at the junction between the duplex repeat and the 3′ G-overhang (Stansel *et al*, 2001); therefore, it is also possible that Topo IIIα is recruited with TRF2 to modulate the t-loop formation. Our experiments do not exclude the requirement for another protein partner to form the complex at telomere. For example, other proteins of the shelterin complex, including POT1 and TPP1, are also recruited to the telomeric G-overhang (Wang *et al*, 2007; Xin *et al*, 2007) and may modulate the action of Topo IIIα ; finally, BLAP75 was shown to trigger the association of Topo IIIα with DHJ (Wu *et al*, 2006).

Interestingly, the depletion of Topo IIIα leads to a rapid telomere defect in ALT cells but not in telomerase-positive cells. This suggests that Topo IIIα is essential for the ALT pathway of telomere maintenance. In agreement with this hypothesis, the ALT cells depleted in Topo IIIα exhibited severe chromosome segregation defects, a loss of the 3′ telomeric overhang, the induction of TIF, and a reduced expression of TRF2. The reduced protein level of TRF2 upon Topo IIIα knockdown was not observed in telomerase-positive cells, suggesting the existence of quantitative or qualitative difference in TRF2/Topo IIIα interactions between ALT and telomerase-positive cells, in keeping with our observations in immunofluorescence and ChIP experiments.

The depletion of Topo IIIα also leads to a rapid growth defect in ALT cells but not in telomerase-positive cells. Topo IIIα has been initially reported to associate with BLM and is targeted to its DNA substrate by RMI1/BLAP75 (Johnson

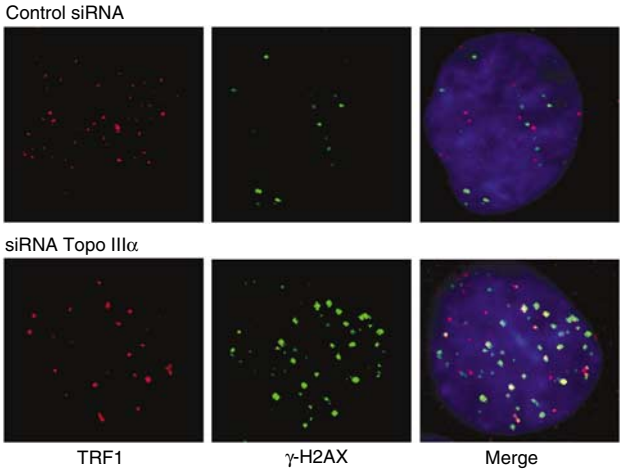

Figure 8 DNA damage response at the telomere after Topo IIIα depletion in U2OS cells. U2OS cells were treated for 48 h with control siRNA or with Si-1 and examined for γ-H2AX foci (green) that colocalized with TRF1 (red).

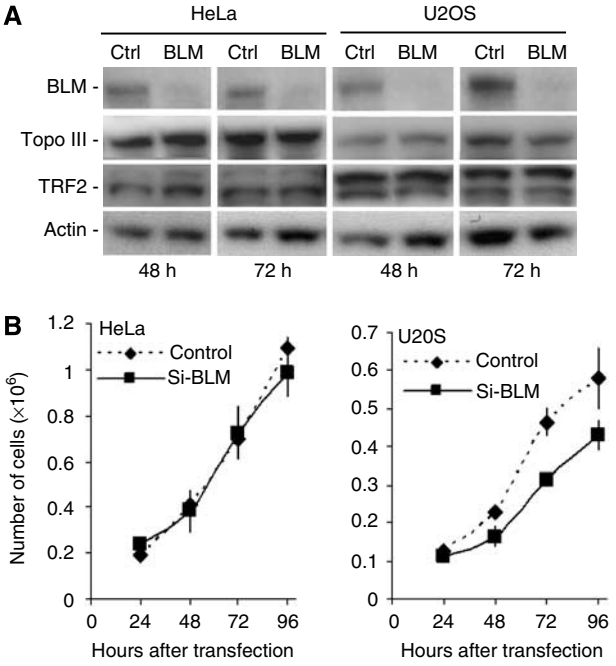

Figure 9 Effect of BLM depletion on Topo IIIα and TRF2 protein levels and on the growth of telomerase-positive cells and ALT cells. (**A**) Western blot analysis of Topo IIIα or TRF2 levels after siRNA-mediated depletion of BLM in HeLa or U2OS cells. Proteins were extracted at the indicated time points after transfection of HeLa or U2OS cells with anti-BLM siRNA (100 nM) or a control siRNA. BLM (upper panel), Topo IIIα, and TRF2 levels were monitored by western blotting using specific antibodies. The membrane was reprobed with anti-β-actin antibody as a loading control (lower panel). (**B**) Effect of BLM depletion (Si-BLM, 100 nM) on the growth of telomerase-positive (HeLa) and ALT (U2OS) cell lines for up to 96 h after transfection. In brief, cells were harvested and counted every 24 h using one well for each time point. Cells were then lysed and sonicated and BLM depletion was monitored by western blot analysis (data not shown). The values represent the mean of two independent experiments and error bars indicate variation.

et al, 2000; Wu *et al*, 2000, 2006; Yin *et al*, 2005). This protein complex participates in the repair of replication defect and in the control of genomic stability. Interestingly, siRNA-mediated depletion of BLM in U2OS cells presented some differences with Topo IIIα depletion. BLM depletion affected less severely the growth of ALT cells but did not affect Topo IIIα and TRF2 protein levels in telomerase-positive or ALT cells, a result consistent with the presence of a stable Topo III/TRF2 complex in BLM-deficient cells (result not shown). In agreement with this, BLAP75 depletion, but not BLM depletion, was found to be essential for the stability of the BLM/Topo III/BLAP75 complex in HeLa cells (Yin *et al*, 2005). These data suggest that the stability of TRF2 specifically depends on the presence of Topo IIIα in ALT cells, but not BLM, even though all three proteins are components of the same complex. It is worth noting that, in contrast to Topo IIIα depletion, a reduced expression of factors possibly involved in ALT usually does not affect short-term cell viability, even when proteins that are essential for telomere maintenance, such as TRF2, are knocked down to very low levels (Jiang *et al*, 2007). Therefore, it is not excluded that the telomere defects are due to the decreased TRF2 whereas the ALT cell proliferation effects are more clearly related to Topo IIIα. This once again confirms the notion that TRF2 and Topo IIIα bear central functions in ALT cells although their exact roles, as compared to telomerase-positive cells, remain to be determined.

In contrast to ALT cells, the growth of telomerase-positive cells was unaffected by siRNA-induced Topo IIIα depletion. Although we cannot exclude that prolonged (>96 h) depletion of Topo IIIα might have a delayed effect on cell growth in telomerase-positive cells, our results are in agreement with data obtained when HeLa cells were treated with a short hairpin RNA that inhibited Topo IIIα expression (Tsai *et al*, 2006). Interestingly, this study also presents the long-term survival and the selection of Saos-2 ALT cell clones where Topo IIIα has been depleted. In contrast to our study, the long-term selection of Saos-2 clones with a mild Topo IIIα depletion (40–60%) led to a disappearance of the ALT phenotype and the reactivation of telomerase activity. It is interesting to note that the positive selection of survivors is associated with a modification of the telomere maintenance whereas our study reveals an alteration of the telomere maintenance associated with a growth defect, therefore highlighting the importance of Topo IIIα for these processes in ALT.

We propose that Topo IIIα depletion in ALT cells results in a rapid accumulation of unresolved, post-replicative, recombination intermediates leading to abnormal mitosis and growth arrest. This model is consistent with the recent observations that BLM and Topo IIIα are involved in sister chromatid disjunction after the onset of anaphase (Chan *et al*, 2007) and with the finding of a specifically phosphorylated form of BLM that associates with Topo IIIα during mitosis (Dutertre *et al*, 2002). The telomere–telomere recombination or telomere–ECTR recombination that occurs in ALT may explain the requirement of Topo IIIα to decatenate DHJ and to allow the termination of homologous recombination. In the absence of Topo IIIα, a classical Holliday junction resolution pathway (Wu and Hickson, 2006) may lead to a DNA damage response and disrupt telomere ends. Alternatively, these additional defects might result from the partial loss of TRF2 triggered by Topo IIIα knockdown. Our results suggest that the Topo IIIα/BLM/TRF2 complex is involved in the maintenance of telomere stability and the recombination

processes taking place at the extremities of telomeres of ALT cells.

Materials and methods

Plasmids

Full-length hTRF2 and TIN2 cDNA were cloned into pCDNA3.1 vector (Invitrogen, Carlsbad, CA) by PCR using the Marathon testis cDNA library (Clontech, Palo Alto, CA). The cDNA was completely sequenced and corresponded to the sequence previously released. The CFP–TRF2 plasmid was constructed by insertion of the TRF2 cDNA after PCR amplification from pCDNA3.1-TRF2 vector at the *Bam*HI–*Xba*I site in the pECFP-C1 plasmid. The CFP–TIN2 plasmid was constructed by insertion of the TIN2 cDNA after PCR amplification from pCDNA3.1-TIN2 vector at the *Bam*HI–*Xba*I site in the pECFP-C1 plasmid. Full-length hPOT1 was previously cloned into the pET22b expression vector by PCR using the Marathon testis cDNA library (Clontech) (Gomez *et al*, 2006a). The CFP–POT1 plasmid was constructed by insertion of the POT1 cDNA from the pET22bPOT1 vector at the *Bam*H1–*Xba*1 site of the pECFP-C1 plasmid (Clontech). Full-length Topo IIIα cDNA was cloned previously into pET29H2 (Goulaouic *et al*, 1999). The YFP–Topo IIIα plasmid was constructed by insertion of the Topo IIIα cDNA after PCR amplification and enzymatic digestion from pET29H2-Topo IIIα vector at the *Bam*HI–*Xba*I site in the pEYFP-N1 plasmid.

Cell culture and transfection

EcR293 (Invitrogen), HT1080, 293T (ATCC), MRC5-V1 (a gift from F Megnin-Chanet, Institut Curie, Orsay; Huschtscha and Holliday, 1983), U2OS (ATCC), HeLa, and WI38-VA13 (ATCC) were grown in Dulbecco's modified Eagle's medium (GIBCO from Invitrogen) supplemented with 10% (v/v) fetal bovine serum (Invitrogen), 100 u of penicillin, and 0.1 mg of streptomycin per ml. The GM08505 cell line is a BLM-deficient, SV40-transformed fibroblast cell line that contains a homozygous frameshift mutation in BLM (Ellis *et al*, 1995); these cells were grown in DMEM supplemented with 20% SVF and antibiotics (as specified above). Transfection experiments were carried out according to previously described protocols (Gomez *et al*, 2006a). MRC5-V1, HT1080, and EcR293 were stably transfected with YFP–Topo III vector or MRC5-V1 were cotransfected with YFP–Topo III and CFP constructs (TIN2, POT1, or TRF2). After transfection, cells were selected for 15 days with 400 μg/ml of geneticin and cultures were sorted by FACS analysis and further grown in the presence of 400 μg/ml geneticin.

siRNA experiments

Double-stranded siRNAs were generated to target human Topo IIIα mRNA (NM004618) at nucleotides 462 (5′-ACAUCGGGUUUGAGA UUAU-3′, Si-1), 788 (5′-CCAGAAAUCUUCCACAGAA-3′, Si-2), and 1798 (5′-GGACAAAUUUGUGGUUCUA-3′, Si-3). Control siRNA was purchased from Eurogentec (Belgium). Cells were transfected with 100 nM of siRNA duplex using Lipofectamine 2000 (Invitrogen) without antibiotics and fetal serum (according to the protocol supplied by the manufacturer), at 3×10^5, 4×10^5, 2.5×10^5, 1×10^5, and 6×10^4 cells per 9.5 cm^2 culture dish for EcR293, HT1080, MRC5-V1, U2OS, and WI38-VA13, respectively. HT1080 cells were split at 24 h to avoid confluence issues. Cells were counted and viability was determined by Trypan blue exclusion every 24 h using one well for each time point.

For BLM-specific siRNA treatment, U2OS or HeLa cells were used to seed six-well plates ($2–3 \times 10^5$ cells/well) and were transiently transfected with 100 nM of a BLM-specific siRNA pool (Dharmacon) or nonspecific control siRNA (ON-TARGETplus siCONTROL Non-targeting Pool, Dharmacon), using DharmaFECT I^{TM}, according to the manufacturer's instructions.

Antibodies and western blots

Primary antibodies used in this work were raised against PML (PG-M3, mouse, sc-966; Santa Cruz Biotechnology, Santa Cruz, CA), TRF2 (4A794, mouse; Upstate Biotechnology, Lake Placid, NY, USA), BLM (C18, sc-7790; Santa Cruz Biotechnology), β-actin (clone AC-15, mouse; Sigma, St Louis, MO), active caspase-3 (IMG-144, mouse; Imgenex, San Diego, CA), cleaved PARP (Asp214, rabbit; Cell Signaling Technology, Boston, MA), α-tubulin (clone B-5-1-2, mouse; Sigma), γ-H2AX (mouse; Upstate Biotechnology), TRF1 (C19, goat, sc-1977; Santa Cruz Biotechnology), and Topo IIIα (clone D6, rabbit; Wu *et al*, 2000). Secondary antibodies used for western blot experiments were goat anti-rabbit and anti-mouse HRP conjugates (Upstate Biotechnology) and donkey anti-goat HRP conjugates (Abcam, Cambridge, UK). For immunofluorescence experiments, goat anti-mouse Alexa fluor 488 and 568 as well as goat anti-rabbit Alexa fluor 568 (Invitrogen) were used. Immunoblotting was performed according to Douarre *et al* (2005) and autoradiographs were scanned and quantified using the ImageQuant software (GE Healthcare, Munich, Germany).

Co-immunoprecipitation analysis

The protein extract was prepared from 175 cm^2 dishes ($20–30 \times 10^6$ cells) for each cell line using RIPA buffer complemented with protease inhibitor cocktail (Complete, Mini, EDTA-free; Roche Applied Science, Indianapolis, IN) and 330 mM NaCl. The extract was precleared by protein G-Sepharose 4 Fast Flow (GE Healthcare) for 10 min at 4°C. For immunoprecipitation, precleared nuclear extract (5 mg/ml) was mixed with the required antibody or with control IgG for the negative control. After the tubes were rotated overnight at 4°C, 100 μl of protein G-Sepharose beads (settled volume) was added to each sample and the tubes were rotated for another night at 4°C. The beads were collected by centrifugation and washed three times with PBS buffer, eluted with Laemmli loading buffer, and analysed by immunoblotting as described previously (Dutertre *et al*, 2002; Douarre *et al*, 2005).

Chromatin immunoprecipitations

ChIP was performed according to the manufacturer's instructions (Upstate Biotechnology). Dot blot experiments were performed according to Verdun *et al* (2005), using a 650 bp telomeric insert prepared from pUCTelo plasmid and a 100 bp ALU probe prepared by PCR amplification according to Walker *et al* (2003). Alternatively, telomeric sequences in immunoprecipitates were amplified by PCR according to Cawthon (2002).

G-overhang hybridization assays

The nondenaturing hybridization assay to detect the 3′ telomeric G-overhang was performed as described previously using the $(AATCCC)_4$ oligonucleotide (Gomez *et al*, 2006b).

Immunofluorescence

Immunofluorescence was performed according to Gomez *et al* (2006a), except that α-tubulin staining was as described by Dodson *et al* (2004). We obtained images of fixed cells using a × 100 (NA 1.4) plan apochromat objective mounted on a piezo translator (Physik Instrumente, Karlsruhe, Germany) and imaged with a Coolsnap HQ camera controlled by Metamorph software (Roper Scientific, Duluth, GA). Appropriate excitation and emission filters placed in two filter wheels driven by a Lambda 10-2 controller (Sutter Instruments, Novato, CA) were combined to specific double- or triple-band dichroic filters (Chroma Technology, Rockingham, VT). Stacks of 60–100 images (16-bit greyscale) were acquired with a z-step of 0.12 μm with a low illumination intensity to avoid photobleaching. For data processing, experimental point spread functions were obtained from infra-resolution fluorescent microspheres emitting at specific wavelengths (Molecular Probes), whose stacks were acquired in the same sampling conditions as those used for the volumes to be analysed. Deconvolution was performed with Metamorph software on a 2.4-GHz Dell computer equipped with a GeForce4 Ti 4800 Se Winfast A280 video card (Leadtek Research Inc., Almere, The Netherlands).

Electrophoretic mobility shift assay

EMSA using Topo IIIα was performed on a telomeric substrate with a 3′ G-overhang (Tel-1) and without a 3′ G-overhang (Tel-2) according to Amiard *et al* (2007). Topo IIIα was purified according to Goulaouic *et al* (1999). Sequences used were as follows: Tel1-G 5′-ATCGTCCTAGCAAGGGTTAGGGTTAGGGTTAGGGTTAGGGTTAG GGTTAGGGTTAGGGTTA-3′, Tel1-C 5′-CTAACCCTAACCCTAACCCTA ACCCCTTGCTAGGACGAT-3′, Tel2-G 5′-GGCTGCTACCGGCACATCG TCCTAGCAAGGTTAGGGTTAGGGTTAGGGTTAGGG-3′, Tel2-C 5′-CC CTAACCCTAACCCTAACCCTAACCTTGCTAGGACGATGTGCCGGTAGC AGCC-3′ The G-strands, Tel1-G or Tel2-G, were labelled at the 5′ end by [γ-^{32}P]ATP using T4 kinase and purified. Tel1-C and Tel2-C were annealed overnight at 80°C with their respective G-strand, run on polyacrylamide gel, and purified.

Supplementary data
Supplementary data are available at *The EMBO Journal* Online (http://www.embojournal. org).

Acknowledgements

We thank H Goulaouic, P Mailliet, R Onclercq-Delic̀, G Labarchede-Buhagiar, JL Mergny, C Trentesaux, H Morjani, P Arimondo, and C Morrisson for useful discussions and scientific collaborations. This work was supported by the 'Ligue Nationale contre le Cancer, Equipes labellisées' for J-FR and EG, by an European Union FP6 grant (LSHC-CT–2004-502943) and by the 'Institut National du Cancer' for MAG. TW and NT-S were supported by fellowship from the 'Région Champagne-Ardenne'. CD is supported by a fellowship from 'Association pour la Recherche contre le Cancer'. LG and EB are supported by a fellowship from the 'Ligue Nationale contre le Cancer'.

References

Ababou M, Dutertre S, Lecluse Y, Onclercq R, Chatton B, Amor-Gueret M (2000) ATM-dependent phosphorylation and accumulation of endogenous BLM protein in response to ionizing radiation. *Oncogene* **19:** 5955–5963

Amiard S, Doudeau M, Pinte S, Poulet A, Lenain C, Faivre-Moskalenko C, Angelov D, Hug N, Vindigni A, Bouvet P, Paoletti J, Gilson E, Giraud-Panis MJ (2007) A topological mechanism for TRF2-enhanced strand invasion. *Nat Struct Mol Biol* **14:** 147–154

Amor-Gueret M (2006) Bloom syndrome, genomic instability and cancer: the SOS-like hypothesis. *Cancer Lett* **236:** 1–12

Cawthon RM (2002) Telomere measurement by quantitative PCR. *Nucleic Acids Res* **30:** e47

Cesare AJ, Griffith JD (2004) Telomeric DNA in ALT cells is characterized by free telomeric circles and heterogeneous t-loops. *Mol Cell Biol* **24:** 9948–9957

Champoux JJ (2001) DNA topoisomerases: structure, function, and mechanism. *Annu Rev Biochem* **70:** 369–413

Chan KL, North PS, Hickson ID (2007) BLM is required for faithful chromosome segregation and its localization defines a class of ultrafine anaphase bridges. *EMBO J* **26:** 3397–3409

Chang M, Bellaoui M, Zhang C, Desai R, Morozov P, Delgado-Cruzata L, Rothstein R, Freyer GA, Boone C, Brown GW (2005) RMI1/NCE4, a suppressor of genome instability, encodes a member of the RecQ helicase/Topo III complex. *EMBO J* **24:** 2024–2033

Chen CF, Brill SJ (2007) Binding and activation of DNA topoisomerase III by the Rmi1 subunit. *J Biol Chem* **282:** 28971–28979

de Lange T (2005) Shelterin: the protein complex that shapes and safeguards human telomeres. *Genes Dev* **19:** 2100–2110

Dodson H, Bourke E, Jeffers LJ, Vagnarelli P, Sonoda E, Takeda S, Earnshaw WC, Merdes A, Morrison C (2004) Centrosome amplification induced by DNA damage occurs during a prolonged G2 phase and involves ATM. *EMBO J* **23:** 3864–3873

Douarre C, Gomez D, Morjani H, Zahm JM, O'Donohue MF, Eddabra L, Mailliet P, Riou JF, Trentesaux C (2005) Overexpression of Bcl-2 is associated with apoptotic resistance to the G-quadruplex ligand 12459 but is not sufficient to confer resistance to long-term senescence. *Nucleic Acids Res* **33:** 2192–2203

Dunham MA, Neumann AA, Fasching CL, Reddel RR (2000) Telomere maintenance by recombination in human cells. *Nat Genet* **26:** 447–450

Dutertre S, Sekhri R, Tintignac LA, Onclercq-Delic R, Chatton B, Jaulin C, Amor-Gueret M (2002) Dephosphorylation and subcellular compartment change of the mitotic Bloom's syndrome DNA helicase in response to ionizing radiation. *J Biol Chem* **277:** 6280–6286

Ellis NA, Groden J, Ye TZ, Straughen J, Lennon DJ, Ciocci S, Proytcheva M, German J (1995) The Bloom's syndrome gene product is homologous to RecQ helicases. *Cell* **83:** 655–666

Gangloff S, McDonald JP, Bendixen C, Arthur L, Rothstein R (1994) The yeast type I topoisomerase Top3 interacts with Sgs1, a DNA helicase homolog: a potential eukaryotic reverse gyrase. *Mol Cell Biol* **14:** 8391–8398

Gomez D, O'Donohue MF, Wenner T, Douarre C, Macadre J, Koebel P, Giraud-Panis MJ, Kaplan H, Kolkes A, Shin-ya K, Riou JF (2006a) The G-quadruplex ligand telomestatin inhibits POT1 binding to telomeric sequences *in vitro* and induces GFP-POT1 dissociation from telomeres in human cells. *Cancer Res* **66:** 6908–6912

Gomez D, Wenner T, Brassart B, Douarre C, O'Donohue MF, El Khoury V, Shin-Ya K, Morjani H, Trentesaux C, Riou JF (2006b) Telomestatin-induced telomere uncapping is modulated by POT1 through G-overhang extension in HT1080 human tumor cells. *J Biol Chem* **281:** 38721–38729

Goulaouic H, Roulon T, Flamand O, Grondard L, Lavelle F, Riou JF (1999) Purification and characterization of human DNA topoisomerase IIIalpha. *Nucleic Acids Res* **27:** 2443–2450

Grobelny JV, Godwin AK, Broccoli D (2000) ALT-associated PML bodies are present in viable cells and are enriched in cells in the G(2)/M phase of the cell cycle. *J Cell Sci* **113** (Part 24)**:** 4577–4585

Hickson ID (2003) RecQ helicases: caretakers of the genome. *Nat Rev Cancer* **3:** 169–178

Huang P, Pryde FE, Lester D, Maddison RL, Borts RH, Hickson ID, Louis EJ (2001) SGS1 is required for telomere elongation in the absence of telomerase. *Curr Biol* **11:** 125–129

Huschtscha LI, Holliday R (1983) Limited and unlimited growth of SV40-transformed cells from human diploid MRC-5 fibroblasts. *J Cell Sci* **63:** 77–99

Jiang WQ, Zhong ZH, Henson JD, Reddel RR (2007) Identification of candidate alternative lengthening of telomeres genes by methionine restriction and RNA interference. *Oncogene* **26:** 4635–4647

Johnson FB, Lombard DB, Neff NF, Mastrangelo MA, Dewolf W, Ellis NA, Marciniak RA, Yin Y, Jaenisch R, Guarente L (2000) Association of the Bloom syndrome protein with topoisomerase IIIalpha in somatic and meiotic cells. *Cancer Res* **60:** 1162–1167

Kim RA, Caron PR, Wang JC (1995) Effects of yeast DNA topoisomerase III on telomere structure. *Proc Natl Acad Sci USA* **92:** 2667–2671

Lenain C, Bauwens S, Amiard S, Brunori M, Giraud-Panis MJ, Gilson E (2006) The Apollo 5′ exonuclease functions together with TRF2 to protect telomeres from DNA repair. *Curr Biol* **16:** 1303–1310

Lillard-Wetherell K, Machwe A, Langland GT, Combs KA, Behbehani GK, Schonberg SA, German J, Turchi JJ, Orren DK, Groden J (2004) Association and regulation of the BLM helicase by the telomere proteins TRF1 and TRF2. *Hum Mol Genet* **13:** 1919–1932

Londono-Vallejo JA, Der-Sarkissian H, Cazes L, Bacchetti S, Reddel RR (2004) Alternative lengthening of telomeres is characterized by high rates of telomeric exchange. *Cancer Res* **64:** 2324–2327

Mao Z, Seluanov A, Jiang Y, Gorbunova V (2007) TRF2 is required for repair of nontelomeric DNA double-strand breaks by homologous recombination. *Proc Natl Acad Sci USA* **104:** 13068–13073

McEachern MJ, Krauskopf A, Blackburn EH (2000) Telomeres and their control. *Annu Rev Genet* **34:** 331–358

Mergny JL, Riou JF, Mailliet P, Teulade-Fichou MP, Gilson E (2002) Natural and pharmacological regulation of telomerase. *Nucleic Acids Res* **30:** 839–865

Nabetani A, Yokoyama O, Ishikawa F (2004) Localization of hRad9, hHus1, hRad1, and hRad17 and caffeine-sensitive DNA replication at the alternative lengthening of telomeres-associated promyelocytic leukemia body. *J Biol Chem* **279:** 25849–25857

Nitiss JL (1998) Investigating the biological functions of DNA topoisomerases in eukaryotic cells. *Biochim Biophys Acta* **1400:** 63–81

Opresko PL, Mason PA, Podell ER, Lei M, Hickson ID, Cech TR, Bohr VA (2005) POT1 stimulates RecQ helicases WRN and BLM to unwind telomeric DNA substrates. *J Biol Chem* **280:** 32069–32080

Rao VA, Fan AM, Meng L, Doe CF, North PS, Hickson ID, Pommier Y (2005) Phosphorylation of BLM, dissociation from topoisomerase IIIalpha, and colocalization with gamma-H2AX after topoisomerase I-induced replication damage. *Mol Cell Biol* **25:** 8925–8937

Stansel RM, de Lange T, Griffith JD (2001) T-loop assembly *in vitro* involves binding of TRF2 near the 3′ telomeric overhang. *EMBO J* **20:** 5532–5540

Tsai HJ, Huang WH, Li TK, Tsai YL, Wu KJ, Tseng SF, Teng SC (2006) Involvement of topoisomerase III in Telomere–telomere recombination. *J Biol Chem* **281:** 13717–13723

van Overbeek M, de Lange T (2006) Apollo, an Artemis-related nuclease, interacts with TRF2 and protects human telomeres in S phase. *Curr Biol* **16:** 1295–1302

Verdun RE, Crabbe L, Haggblom C, Karlseder J (2005) Functional human telomeres are recognized as DNA damage in G2 of the cell cycle. *Mol Cell* **20:** 551–561

Walker JA, Kilroy GE, Xing J, Shewale J, Sinha SK, Batzer MA (2003) Human DNA quantitation using Alu element-based polymerase chain reaction. *Anal Biochem* **315:** 122–128

Wallis JW, Chrebet G, Brodsky G, Rolfe M, Rothstein R (1989) A hyper-recombination mutation in *S. cerevisiae* identifies a novel eukaryotic topoisomerase. *Cell* **58:** 409–419

Wang F, Podell ER, Zaug AJ, Yang Y, Baciu P, Cech TR, Lei M (2007) The POT1–TPP1 telomere complex is a telomerase processivity factor. *Nature* **445:** 506–510

Wang JC (1996) DNA topoisomerases. *Annu Rev Biochem* **65:** 635–692

Wang JC (2002) Cellular roles of DNA topoisomerases: a molecular perspective. *Nat Rev Mol Cell Biol* **3:** 430–440

Wang RC, Smogorzewska A, de Lange T (2004) Homologous recombination generates T-loop-sized deletions at human telomeres. *Cell* **119:** 355–368

Wang W, Seki M, Narita Y, Sonoda E, Takeda S, Yamada K, Masuko T, Katada T, Enomoto T (2000) Possible association of BLM in decreasing DNA double strand breaks during DNA replication. *EMBO J* **19:** 3428–3435

Wu L, Bachrati CZ, Ou J, Xu C, Yin J, Chang M, Wang W, Li L, Brown GW, Hickson ID (2006) BLAP75/RMI1 promotes the BLM-dependent dissolution of homologous recombination intermediates. *Proc Natl Acad Sci USA* **103:** 4068–4073

Wu L, Davies SL, North PS, Goulaouic H, Riou JF, Turley H, Gatter KC, Hickson ID (2000) The Bloom's syndrome gene product interacts with topoisomerase III. *J Biol Chem* **275:** 9636–9644

Wu L, Hickson ID (2001) RecQ helicases and topoisomerases: components of a conserved complex for the regulation of genetic recombination. *Cell Mol Life Sci* **58:** 894–901

Wu L, Hickson ID (2002) The Bloom's syndrome helicase stimulates the activity of human topoisomerase IIIalpha. *Nucleic Acids Res* **30:** 4823–4829

Wu L, Hickson ID (2003) The Bloom's syndrome helicase suppresses crossing over during homologous recombination. *Nature* **426:** 870–874

Wu L, Hickson ID (2006) DNA helicases required for homologous recombination and repair of damaged replication forks. *Annu Rev Genet* **40:** 279–306

Xin H, Liu D, Wan M, Safari A, Kim H, Sun W, O'Connor MS, Songyang Z (2007) TPP1 is a homologue of ciliate TEBP-beta and interacts with POT1 to recruit telomerase. *Nature* **445:** 559–562

Yankiwski V, Marciniak RA, Guarente L, Neff NF (2000) Nuclear structure in normal and Bloom syndrome cells. *Proc Natl Acad Sci USA* **97:** 5214–5219

Yeager TR, Neumann AA, Englezou A, Huschtscha LI, Noble JR, Reddel RR (1999) Telomerase-negative immortalized human cells contain a novel type of promyelocytic leukemia (PML) body. *Cancer Res* **59:** 4175–4179

Yin J, Sobeck A, Xu C, Meetei AR, Hoatlin M, Li L, Wang W (2005) BLAP75, an essential component of Bloom's syndrome protein complexes that maintain genome integrity. *EMBO J* **24:** 1465–1476

